Articles

Vinyldeoxyadenosine in a Sarcin−Ricin RNA Loop and Its Binding to Ricin Toxin A-Chain†

Setu Roday, Suwipa Saen-oon, and Vern L. Schramm*

Department of Biochemistry, Albert Einstein College of Medicine, 1300 Morris Park Avenue, Bronx, New York 10461

Received October 20, 2006; Revised Manuscript Received March 8, 2007

ABSTRACT: 8-Vinyl-2′-deoxyadenosine (8vdA) is a fluorophore with a quantum yield comparable to that of 2-aminopurine nucleoside. 8vdA was incorporated into a 10-mer stem−tetraloop RNA (8vdA-10) structure for characterization of the properties of the base, 8-vinyladenine (8-vA), with respect to adenine as a substrate or inhibitor for ribosome-inactivating proteins. Ricin toxin A-chain (RTA) and pokeweed antiviral protein (PAP) catalyze the release of adenine from a specific adenosine on a stem−tetraloop (GAGA) sequence at the elongation factor (eEF2) binding site of the 28S subunit of eukaryotic ribosomes, thereby arresting translation. RTA does not catalyze the release of 8-vinyladenine from 8vdA-10. Molecular dynamics simulations implicate a role for Arg180 in oxacarbenium ion destabilization and the lack of catalysis. However, 8vdA-10 is an active site analogue and inhibits RTA with a K_i value of 2.4 μM. Adenine is also released from the second adenosine in the modified tetraloop, demonstrating an alternative mode for the binding of this motif in the RTA active site. The 8vdA analogue defines the specificities of RTA for the two adenylate depurination sites in a RNA substrate with a GAGA tetraloop. The rate of nonenzymatic acid-catalyzed solvolysis of 8-vinyladenine from the stem−loop RNA is described. Unlike RTA, PAP catalyzes the slow release of 8-vinyladenine from 8vdA-10. The isolation of 8-vA and its physicochemical characterization is described.

Ricin is a protein found in castor beans, and it inhibits protein synthesis in eukaryotes by depurination of ribosomes at a site where elongation factors bind during translation (*1*−*4*). The B-chain of this heterodimeric protein is a lectin that directs the catalytic A-chain to the cell surface. Disulfide bond cleavage releases the A-chain which is then internalized via endocytosis (*5*). Once the protein is inside the cell, retrograde transport shuttles it to the endoplasmic reticulum (*6*). The A-chain is then translocated into the cytosol wherein it binds to a GAGA nucleotide sequence on the sarcin−ricin tetraloop (SRL) of the 28S ribosomal RNA and specifically depurinates the first adenosine (A_{4324} on the rat ribosome; $GA_{4324}GA$ in the 5′ → 3′ direction) (Figure 1). The k_{cat} for RTA[1] activity on rat liver ribosomes is ∼1800 min^{-1}, and a single molecule can kill a eukaryotic cell (*7*). A dose of ∼1−2 μg/kg is lethal for dogs. The potency of RTA has been exploited in the assassination of Georgi Markov (*8*)

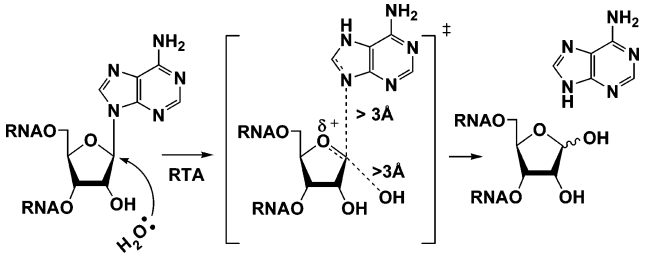

FIGURE 1: Hydrolytic cleavage of a RNA adenosine moiety catalyzed by RTA proceeds through an oxacarbenium ion transition state.

and an attempt on Alexander Solzhenitsyn's life (*9*), these two being the most infamous cases. With a typical content of 10^5−10^7 ribosomes, depurination in a rat hepatocyte would be complete in ∼40 h which is consistent with the rate of fatal ricin poisoning. RTA more recently has also been used as a bioterrorism agent. Inhalation of aerosolized ricin causes rapid and irreversible pulmonary dysfunction. Reliable means of detection (*10*) and the development of antidotes (*11*) are important areas of research for this toxin.

The activity of RTA on small 10−14-mer stem−tetraloop RNA substrates at acidic pH has been demonstrated (*12*), and the k_{cat} for the hydrolysis of 2′-deoxyadenosine in a hybrid GdAGA tetraloop was determined to be ∼16 fold faster than that for an adenosine tetraloop (*13*). Kinetic isotope effects (KIEs) on the hydrolysis of an appropriately radiolabeled 10-mer RNA substrate indicate that the reaction

† Supported by NIH Grant CA7244.

* To whom correspondence should be addressed. E-mail: vern@aecom.yu.edu. Telephone: (718) 430-2813. Fax: (718) 430-8565.

[1] Abbreviations: 8vdA, 8-vinyl-2′-deoxyadenosine; 8-vA, 8-vinyladenine; 8vdA-10, 8vdA incorporated into a 10-mer stem−loop RNA with the sequence 5′-CGCG8vdAGAGCG-3′; 8vAde, 8-vinyladenosine; RTA, ricin toxin A-chain; PAP, pokeweed antiviral protein; KIEs, kinetic isotope effects; A-10, stem−loop RNA with the sequence 5′-CGCGAGAGCG-3′; A-14, stem−loop RNA with the sequence 5′-CGCGCGAGAGCGCG-3′; ApG, adenyl-3′,5′-guanosine; vApG, 8-vinyladenyl-3′,5′-guanosine; dApG, 2′-deoxyadenyl-3′,5′-guanosine; vdApG, 2′-deoxy-8-vinyladenyl-3′,5′-guanosine.

10.1021/bi0621821 CCC: $37.00
Published on Web 05/04/2007

proceeds through a dissociative transition state (TS) (*14*). TS formation at the RTA active site involves leaving group activation, oxacarbenium ion formation, and generation of the insipient water nucleophile. Leaving group activation is the major driving force for catalysis. We hypothesized that the incorporation of 8-vinyl-2′-deoxyadenosine into a RNA 10-mer structure could provide a useful fluorescent substrate or an inhibitor of RTA. It is likely that the vinyl moiety, with its ability to delocalize electrons, makes 8-vA a better leaving group than adenine. If 8-vA were released, the reaction would become amenable to direct spectroscopic characterization and thus yield a continuous assay system. If not a substrate, a RNA construct with 8-vA could inhibit RTA and provide useful information in the design of inhibitors. The following sections describe the incorporation of the vinyl nucleoside into RNA, the binding of the modified stem−loop sequence to RTA, and a molecular dynamics interpretation of the interaction.

EXPERIMENTAL PROCEDURES

Materials and General Experimental. RTA was purchased from Sigma. Pokeweed antiviral protein was purchased from Worthington Biochemicals. Calf intestinal alkaline phosphatase was from Promega (Madison, WI), and phosphodiesterase I was from Sigma Chemical Co. (St. Louis, MO). RNase inhibitors and RNase-free DNase were from Ambion (Austin, TX). Nucleoside phosphoramidites and other reagents for oligoribonucleotide synthesis were purchased from Glen Research (Sterling, VA), except for phosphoramidites attached directly to CPG solid supports, which were obtained from ChemGene Corp. (Ashland, MA). All other chemicals were purchased from Aldrich Chemical Co. (Milwaukee, WI) and were of the highest available purity. These reagents were used without further purification. Purification of reaction intermediates of the phosphoramidite synthetic pathway was completed by flash column chromatography using Merck silica gel 60 (230−400 mesh). Purification by HPLC was performed on a Waters 626 pump with either a 996 photodiode array detector or a 487 dual-wavelength detector and using the Millennium software package. RNA concentrations were determined by UV−vis measurements using a Cary 100 or 300 diode array spectrophotometer from Varian.

Synthesis of the 8-Vinyl-2′-deoxyadenosine Phosphoramidite. The synthesis of the vinyl phosphoramidite was carried out as reported by Mély et al. (*15*). This phosphoramidite can be purchased from Berry and Associates, Inc. However, at the beginning of our work and through the completion of the synthesis, this product was not commercially available.

Synthesis and Purification of 8vdA-10. The oligonucleotide was chemically synthesized using a phosphoramidite methodology on an Expedite 8900 Nucleic Acid Synthesis System from Perseptive Biosystems. Syntheses were carried out on a 1 μmol scale with coupling times extended to 15 min, in the trityl-off mode. The coupling times for guanosine and 8-vinyl-2′-deoxyadenosine were extended to 40 min. Deprotection of the products was accomplished using a concentrated NH_4OH/ethanol mixture (3:1, v/v) and triethylamine trihydrofluoride as described by Chen et al. (*12*) All products were purified by HPLC using a Waters XTerra Prep MS C18 column (7.8 mm × 50 mm). These columns are specially designed for purification of oligonucleotides in the trityl-off mode. An ion pairing mobile phase of 50 mM triethylammonium carbonate (pH 6.4) with a gradient from 3 to 80% of 50% methanol was employed for elution. The homogeneity of the product was confirmed by ion exchange chromatography on a Protein-Pak Q-15 HR DEAE column eluting with 50 mM ammonium acetate (pH 5.0) containing 15% methanol and 1.0 M LiCl. The nucleotide composition was confirmed by enzymatic digestion of a 50 μL aliquot of a 2.5 μM solution of the oligonucleotide with 1 unit each of calf intestinal alkaline phosphatase and snake venom phosphodiesterase I overnight at 37 °C, and quantitation of the released nucleosides relative to known standards by HPLC on a Waters Delta-Pak C18 analytical column (3.9 mm × 300 mm) eluted with 50 mM ammonium acetate (pH 5.0) containing 5% methanol. Nucleoside and deoxynucleoside standards were used to determine the relative amounts of each component in the digest. Product formation was further confirmed by MALDI-TOF mass spectrometry analysis on an Applied Biosystems 4115 Voyager system. Masses were acquired in the 500−5000 Da range.

Synthesis and Purification of 8-Vinyladenine. 8-Vinyladenine was isolated from an intermediate of the phosphoramidite synthesis pathway. Thus, a solution of 25 mg of 5′-dimethoxytrityl-6-*N*,*N*-dimethylformamidino-8-vinyl-2′-deoxyadenosine in 10 mL of 15% dichloroacetic acid in dichloromethane was allowed to stir at room temperature for 3 h. The solvent was then removed in vacuo, and the residue was dissolved in 5 mL of a 1:1 solution of triethylamine in methanol and stirred at room temperature for 24 h. The solvent was then removed in vacuo, and the crude material was purified by HPLC on a Waters C18 Deltapak analytical column (3 mm × 300 mm) eluting with 50 mM ammonium acetate (pH 5.0) and a gradient from 3 to 80% of 50% methanol over 40 min. The collected fractions were pooled, concentrated, and finally desalted using a C18 zip-tip prior to ESI mass analysis in the negative mode: ^{1}H NMR (CD_3OD, 300 MHz) δ 5.9 (d, J = 11.3 Hz, 1H, cis-vinyl), 6.45 (d, J = 17.7 Hz, 1H, trans-vinyl), 6.95 (dd, J = 11.3 Hz, J = 17.7 Hz, 1H, vinyl), 8.35 (s, 1H, C2-H); calcd mass 161.07, observed mass 160.0.

Synthesis and Purification of 8-Vinyladenosine. The synthesis of 8-vinyladenosine was carried out as reported by Manfredini et al. (*16*).

Kinetic Experiments. Reaction rates with RTA were determined in 10 mM potassium citrate buffer (pH 4.0) containing 1 mM EDTA. The total reaction volume was 100 μL. Reactions were started by the addition of RTA at concentrations of 0.5−1 μM. After incubation of the reaction vials at 37 °C for the allotted time, the reactions were quenched by inactivating the enzyme with 500 mM potassium phosphate buffer (pH 8.3, 100 μL of a 1 M solution). The samples were then injected onto a reversed-phase C18 Waters Delta-Pak guard and analytical column (3.9 mm × 300 mm) with isocratic elution in 50 mM ammonium acetate (pH 5.0) containing 5% methanol, at a flow rate of 1 mL/min. The enzyme protein is retained on the guard column under these conditions. The extent of hydrolysis of RNA by RTA or by PAP was measured by quantitating the released adenine by monitoring the peak at 260 nm and using a comparison with standards treated with the same protocol. All substrates that were used and 8vdA-10 were heated to

80 °C for 1 min, cooled on ice, and incubated at 37 °C for 15 min prior to their addition to the assay mix to reduce any variability in the turnover rate that might result from conformational heterogeneity (hairpins vs other forms) in solution. In initial rate experiments, the extent of substrate hydrolysis was less than 15%. Product formation was shown to conform to initial rate conditions for the duration of the assay. Substrate reaction rates were fitted to the Michealis−Menten equation. For 8vdA-10, the binding constant (K_d) was assumed to be equal to the competitive dissociation constant (K_i). The latter was determined by fitting the initial rates to the equation for competitive inhibition, $v = k_{cat}[S]/[[S] + K_m(1 + I/K_i)]$, where v is the initial reaction rate, [S] is the substrate concentration, K_m is the Michaelis constant for the substrate (2.9 μM for the competitive substrate, A-10, under the assay conditions), I is the concentration of 8vdA-10, and k_{cat} is the rate of catalytic turnover at substrate saturation. The concentration of 7 μM used for A-10 in this assay is ~2.5 times above its K_m and is a convenient value for competitive inhibitor analysis (*17*). All reactions with PAP were carried out either in 25 mM HEPES or in 25 mM Tris-HCl buffer at pH 7.8 and 25 °C.

Steady State Fluorescence Measurements. Steady state fluorescence emission spectra of the 8vA-containing oligonucleotide samples were measured on a SPEX Fluoromax spectrofluorometer using a 3 mm square cuvette. The emission spectra were recorded over the wavelength range of 315−450 nm with an excitation wavelength of 305 or 310 nm. The spectral bandpass was 5 nm for all emission spectra. The excitation spectra were recorded over the wavelength range of 240−315 nm by monitoring the emission at 380 nm. Inner filter effects were corrected for the sample concentrations that exhibited a maximal absorbance at the excitation wavelength of >0.1. The concentrations of oligonucleotides used were typically in the range of 2.5−5 μM. The concentrations of 2-aminopurine, 8-vinyladenine, and tryptophan used for measurement of the quantum yield were <1 μM and did not require any correction. Quantum yield values (*18*) were calculated using the equation $\phi_{vA} = \phi_{ref}(I_{vA}/I_{ref})/[10^{(OD_{vA}-OD_{ref})/2}]$, where ϕ_{vA} and ϕ_{ref} are the quantum yields of 8-vinyladenine and the reference sample, respectively, I refers to the integrated emission intensities, and OD represents the optical densities at the excitation wavelength of 305 nm.

Determination of the pK_a of N9 in 8-Vinyladenine. One-dimensional ^{1}H NMR experiments were performed at 25 °C on a Bruker DRX 300 MHz NMR spectrometer equipped with pulsed field gradients. 3-(Trimethylsilyl)propionic-2,2,3,3-d_4 acid sodium salt was used as the internal standard to which the ^{1}H chemical shifts were referenced. A 1 mM solution of 8-vinyladenine in 0.5 mL of D_2O containing 10% CD_3OD as a solubility aid was used in the study. Titrations were performed by adding small aliquots of 0.1 M NaOD or DCl. The pK_a value for N9 of the 8-vinyladenine was determined by following the pH-dependent chemical shift of the CH═CH_2 proton in the vinyl moiety. The apparent electrode readings were not corrected for deuterium isotope effects. The titration data were biphasic, with the chemical shift of the proton in the vinylic system conclusively reporting on the N9 pK_a, whereas the C2 proton reports a pK_a that may correspond to protonation of either N1 or N3. The data were fitted by nonlinear regression analysis to the equation $\delta_{ppm} = \delta_1 + (\Delta\delta_2 \times 10^{pK_{a1}-pH})/(1 + 10^{pK_{a1}-pH}) + (\Delta\delta_3 \times 10^{pK_{a2}-pH})/(1 + 10^{pK_{a2}-pH})$, where δ_{ppm} and δ_1 are the observed chemical shifts at a particular pH and the chemical shift of the unprotonated form, respectively. $\Delta\delta_2$ and $\Delta\delta_3$ represent differences in shifts from the chemical shifts at the low and high limiting pH values, respectively.

Stochastic Deformable Boundary (SDB) Dynamics. The starting structure for the simulations described here was based on the crystal structure of RTA in complex with the dinucleotide, adenyl-3′,5′-guanosine (ApG) (PDB entry 1APG) (*19*). Due to the lack of a crystallographic water molecule in the X-ray structure, an important catalytic water molecule was placed into the active site explicitly. Robertus et al. (*20*) have reported the crystal structure of apo-ricin A- and B-chain at 2.5 Å resolution (PDB entry 2AAI) and identified one water molecule (WAT323) within the active site pocket as the catalytic water forming strong interactions with Glu177 and Arg180. Therefore, we modeled WAT323 into the active site of the RTA−ApG complex. We also modeled 8-vinyladenyl-3′,5′-guanosine (vApG) in complex with the RTA−vApG species using the RTA−ApG complex structure by substituting the C8 position of adenine ring with a vinyl group. 2′-Deoxyadenyl-3′,5′-guanosine (dApG) and the vinyl counterpart, 2′-deoxy-8-vinyladenyl-3′,5′-guanosine (vdApG), were also modeled in a similar fashion.

To investigate the local structural and interaction characteristics of binding of a dinucleotide to the active site of RTA, the stochastic boundary approach (*21*) was applied and all four simulations (RTA−ApG, RTA−vApG, RTA−dApG, and RTA−vdApG) were carried out with CHARMM (*22*). Hydrogen atoms were built using the "hbuild" module in CHARMM. The simulations were run with the truncated protein SDB simulations. The simulation system contained a spherical selection of residues centered around the C1′ atom of adenine dinucleotide. All protein residues with at least one atom within 18 Å of the center were selected. Protein residues outside the spherical zone were held fixed throughout the entire SDB simulation. The systems were then solvated by the superimposition of a 23 Å radius sphere of water (Jorgensen's TIP3P model) (*23*) and deletion of any added water molecule whose oxygen atom was within 2.8 Å of another non-hydrogen atom. One chloride ion was added to neutralize the system. The structure of the model set up for SDB simulation is shown in Figure S1 in the Supporting Information. Water molecules were minimized by applying a harmonic restraint of 10 kcal mol^{-1} Å^2 with 500 steps of steepest descent (SD) minimization. All atoms within the spherical 18 Å radius were then minimized with 500 steps each of steepest descent (SD) and adopted basis Newton Raphson (ABNR) minimization.

All atoms of the system were treated molecular mechanically, using the CHARMM22 all-atom force field. Throughout, a 5 Å buffer zone was defined as all atoms more than 18 Å from the center of the sphere, in which the nonsolvent heavy atoms were harmonically restrained to their crystal coordinates with the force constants. During the dynamics simulations, Langevin dynamics were applied to the buffer region, using friction coefficients of 250 ps^{-1} for non-hydrogen protein atoms and 62 ps^{-1} on water oxygen atoms (*24*). A deformable boundary potential was applied on the water oxygens. Simulations were run with a time step of 1 fs, and the SHAKE algorithm (*25*) with a tolerance of 10^{-8}

was used to constrain all bonds involving hydrogen atoms. Nonbonded interaction energies and forces were smoothly shifted to zero at a cutoff of 12.0 Å by the atom-based truncation method with a force-shifting function. The nonbonded pair list was generated for atoms within a 12 Å cutoff, and the nonbonded list was updated heuristically. The force shift option causing the interaction energies and the force to vanish smoothly at a distance of 10 Å was used. The relative dielectric constant was set to 1.0. Simulation systems were heated from 100 to 300 K over 20 ps. The temperature was progressively increased, and the systems were then equilibrated for 80 ps at 300 K and continued for the production run for a further 300 ps. Trajectories were saved every 10 fs.

RESULTS AND DISCUSSION

Incorporation of 8-Vinyl-2′-deoxyadenosine (8vdA) into RNA. Mély et al. (*15*) have reported the synthesis of 8-vinyl-2′-deoxyadenosine (8vdA) and its phosphoramidite and the subsequent incorporation into DNA. We followed their synthetic route but aimed to incorporate the novel nucleoside phosphoramidite into a small 10-mer stem−tetraloop RNA, 5′-CGCG(8vdA)GAGCG-3′ (8vdA-10). It should be noted, however, that the modified nucleoside is flanked by two guanosines in this sequence and that Mély et al. were only able to incorporate this residue into DNA when the flanking residues were either A, T, or C. When the flanking residue was G, a compound with a mass (ΔM) of +151 was obtained which was consistent with the formation of a guanine adduct. This presumably results from a 1,4-type Michael addition of N7 of the 2′-deoxyguanosine phosphoramidate on the α,β-unsaturated vinyladenine system. In our approach, every residue other than the vinyl nucleoside was a ribonucleoside; thus, the greater inherent acid stability of the guanosine phosphoramidate during RNA synthesis was proposed to decrease the extent of Michael addition. Another concern was the nucleophilic addition of ammonia to the vinyl moiety during deprotection of the DNA from the solid support. This was reduced by allowing the deprotection reaction to proceed for 4 h at room temperature instead of the standard 16−18 h. This problem was also encountered in our initial synthesis but was circumvented by using a 3′-end nucleoside that was derivatized on an oxalyl-controlled pore glass (CPG) solid support (*26*) instead of the standard succinyl-CPG. The former has the advantage of being labile to ammonia-free cleavage with basic reagents like triethylamine which are not nucleophilic. In addition, we used base-labile protecting groups on the C, G, and A residues. 8-Vinyl-2′-deoxyadenosine is both acid labile (hydrolysis of the glycosidic bond) and base susceptible (addition to the vinyl moiety), and thus, care is needed in its exposure time to potentially degradative reagents. A solution of 0.5 M iodine in pyridine is the standard reagent used in DNA synthesis to oxidize the phosphite to the phosphate. In our synthesis of RNA, we replaced this with a solution of 2 M *tert*-butyl hydroperoxide (TBHP) in toluene and dichloromethane (*27*) to prevent exposure of the vinyl moiety to pyridine. We also used 3% dichloroacetic acid in dichloromethane, a mild acid, to effect the removal of the 5′-dimethoxytrityl groups. The synthesis of 8vdA-10 was carried out on a 3 μmole scale with a yield of ∼20%. MALDI mass spectrometry and enzymatic digestion with snake venom phosphodiesterase and alkaline phosphatase confirmed the incorporation of the vinyl nucleoside into the RNA and the composition of the 10-mer species. This is the first report of the incorporation of a vinyl nucleoside into a RNA scaffold.

Fluorescence of 8-Vinyl-2′-deoxyadenosine within the Stem−Loop RNA, 8vdA-10. The emission spectrum of 8vdA in the oligonucleotide 8vdA-10 has a maximum at 388 nm. The quantum yield of the oligonucleotide was determined relative to 2-aminopurine (*28*) and compared with similarly determined quantum yields of 8-vinyl-2′-deoxyadenosine, 8-vinyladenosine, and 8-vinyladenine. The quantum yield of 8vdA-10 was found to be quenched 270-fold relative to that of the vinyl deoxyribonucleoside (Figure 2A,B and Table 1). The spectroscopic behavior of 8vdA in the hairpin RNA is governed by intratetraloop conformational factors. It is known that the "GAGA" tetraloop adopts a structure in solution such that the three purine rings on the 3′-side (i.e., A, G, and A) are stacked upon each other (Figure 2D) (*29*, *30*). A similar conformation is likely for the "G8vdAGA" tetraloop as well and along with the two flanking guanosines explains the dramatic quenching of the vinyl nucleoside fluorescence in the RNA. Further, the emission maximum of the free base, 8-vinyladenine, was found to be at 378 nm (the synthesis of 8-vA is described in a later section) and that of the vinyl nucleosides (both ribo and deoxy) at 384 nm. The 4 nm red shift in the fluorescence of the 8-vinyladenine moiety in RNA suggests that it is solvent-exposed. An examination of the tetraloop structure reveals that the turn in the phosphate backbone between the first guanosine of the loop and the second adenosine (or 8vdA) disposes these residues in spatially different orientations, thus providing solvent accessibility to the first purine of the triple base stack. A study of the temperature dependence of the fluorescence intensity of 8vdA-10 was also carried out (Figure 2C). A 2-fold increase in intensity was observed when the temperature was increased from 22 to 50 °C. The emission maximum was also found to be blue-shifted by 6 nm. The tetraloop is clearly more dynamic at higher temperatures, resulting in an unstacking of the 8-vinyadenine moiety. The disruption of the quenching−stacking effect of the adjacent guanosines at higher temperatures results in the observed changes in fluorescence intensities. At temperatures greater than 60 °C, the 8vdA-10 starts undergoing intrinsic chemical hydrolysis and releases 8-vinyladenine, resulting in a dramatic increase in fluorescence intensity.

The quenching mechanism for 8-vA stacked with A, T, and C has been studied theoretically in dimer and trimer species and compared with the observed quenching of its quantum yield when incorporated into oligonucleotides bearing A, T, or C adjacent to it in the sequence (*31*). However, the quenching mechanism for 8-vA flanked with G was not studied since an oligonucleotide sequence with a G adjacent to 8-vA could not be synthesized. Our successful synthesis of 8vdA-10 with the vinyl nucleoside adjacent to two guanosines and the characterization of its spectral properties in the RNA provide a good experimental oligonucleotide model for comparison with a theoretical analysis of the 8-vA|G quenching mechanism.

Substrate Activity of 8vdA-10 with RTA. 8vdA-10 was tested as a substrate for RTA at pH 4.0 and 37 °C with assay conditions that have been reported previously for stem−loop substrates of RTA (*10*, *11*). The reaction was monitored by

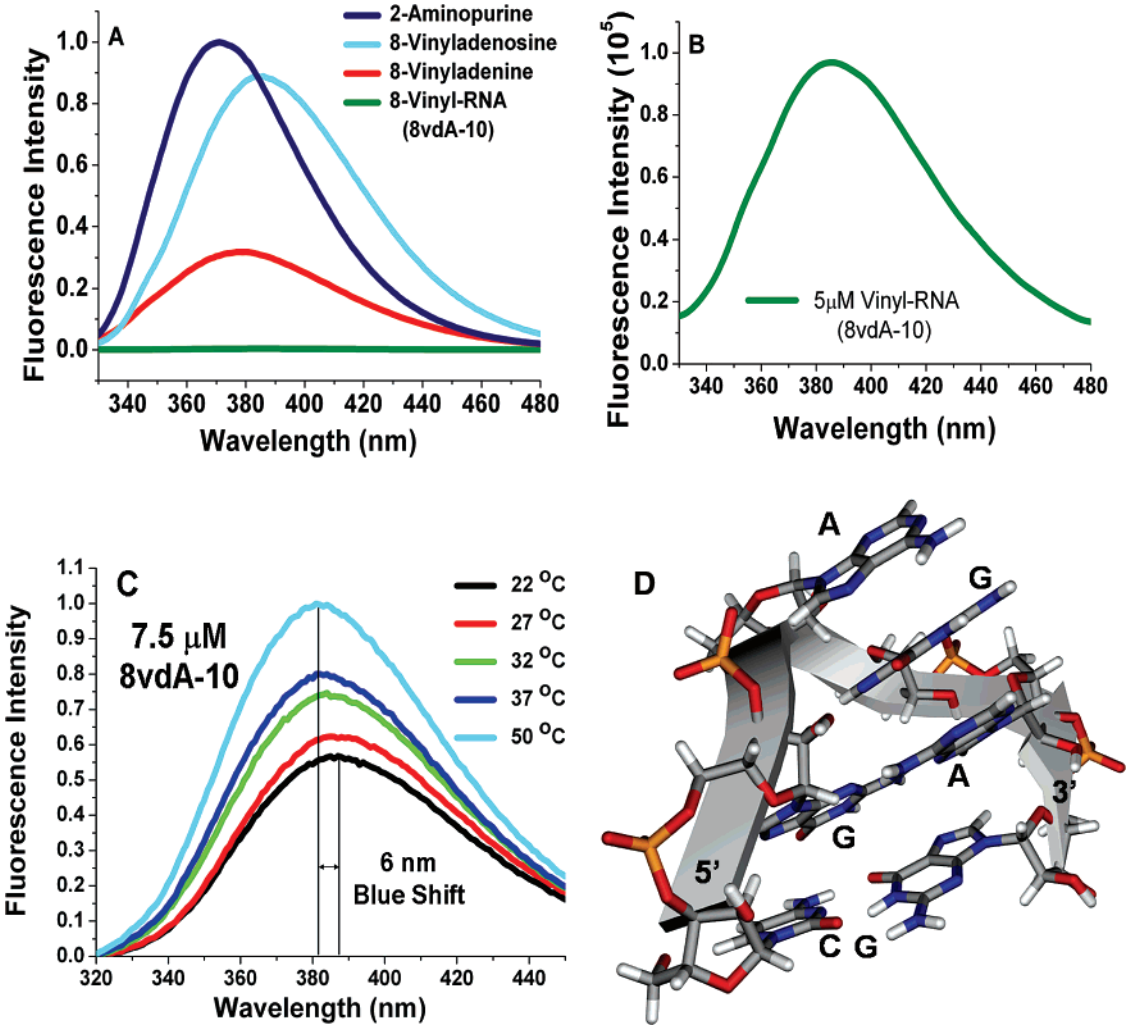

FIGURE 2: (A) Normalized fluorescence intensities of equimolar concentrations of 2-AP, 8vAde, 8vdA, and 8vdA-10 in water at pH 7.0 and 25 °C. (B) Absolute fluorescence intensity of a 5 μM solution of 8vdA-10 in 10 mM phosphate/0.1 mM EDTA buffer at pH 7.1 and 25 °C. (C) Normalized fluorescence intensities of a 7.5 μM solution of 8vdA-10 in 10 mM citrate/0.1 mM EDTA buffer at pH 4.0. (D) Structure of the GAGA tetraloop (PDB entry 1ZIG) (*29*). The tetraloop residues are shown as stick models. Residues A, G, and A on the 3′-side of the loop form a triple-purine stack. The first adenosine on the 5′-side is depurinated by RTA.

Table 1: Relative Quantum Yields of the 8-Vinyl Nucleosides, the Base, and the RNA 10-mer Oligonucleotide Sequence

molecule	λ_{em} (nm)	ϕ
2-aminopurine (2-AP) (*27*)	370	0.66
8-vinyl-2′-deoxyadenosine (8vdA) (*15*)	384	0.68
8-vinyladenosine (8vAde)[a]	384	0.66
8-vinyladenine (8-vA)	378	0.33
8-vinyl-RNA (10-mer, 8vdA-10)	388	0.0025

[a] 8-Vinyladenosine was synthesized using the procedure reported by Manfredini et al. (*16*).

HPLC using dual-wavelength detection at 260 and 305 nm (the λ_{max} of 8vdA is 295 nm). The initial conditions followed the reaction for 1 h at 37 °C. No release of 8-vinyladenine was observed. However, HPLC showed the release of adenine under prolonged conditions (~12 h). A new peak at 305 nm was also observed under these conditions and was assumed to be that of 8-vinyladenine (Figure 3). Control incubations at pH 4.0 without RTA indicated no release of adenine. However, both control and RTA samples released similar amounts of 8-vinyladenine on prolonged incubations, indicating a slow nonenzymatic solvolysis of 8-vinyladenine. Although 8vdA-10 is not a substrate for RTA at the primary depurination site, enzymatic release of adenine from the second site confirms that it binds at the catalytic site. Further, control experiments (10 mM HEPES buffer) at pH 7.0 do not release either adenine or 8-vA upon prolonged incubation. MALDI analysis also established masses corresponding to unreacted RNA, deadenylated RNA, and the devinylated RNA (Figure 3).

RTA catalyzes the specific depurination of the first adenosine in synthetic stem−loop RNA and DNA molecules containing a GAGA tetraloop motif. Chen et al. (*12*) showed that the k_{cat} for the depurination of an all-DNA stem−tetraloop substrate, dA-10, at this site was ~0.38 min^{-1} and the K_m for its binding was ~2.6 μM. Prolonged incubation of dA-10 with RTA caused the release of a second equivalent of adenine as a result of both 2′-deoxyadenosine residues in the DNA tetraloop being hydrolyzed by RTA. The kinetic constants of depurination at the second site were determined using a DNA 10-mer, dR-10, where an abasic residue, 1,2-dideoxy-D-ribose, was substituted for the first dA in the d(GAGA) tetraloop (*32*). The k_{cat} for depurination at the second site (k_1) was ~0.46 min^{-1}, and the K_m was ~160 μM. Chen et al. determined the specificity constant, k_{cat}/K_m, for depurination at the second site to be ~60-fold lower than that at the first. However, this experiment does not provide

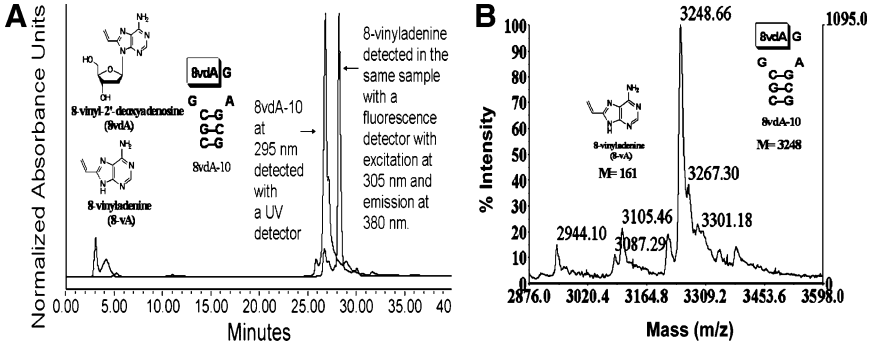

FIGURE 3: (A) HPLC profile of 8vdA-10 upon incubation at 37 °C for 12 h in 10 mM citrate buffer (pH 4.0). The peak at 27 min corresponds to the RNA (8vdA-10), and the peak at 29 min corresponds to 8-vinyladenine. The latter could not be detected at 260 nm. However, it can be detected either at 305 nm (where the sensitivity of detection is ~40 picomoles) or by a fluorescence detector set at an excitation wavelength of 305 nm and an emission wavelength of 380 nm. (B) MALDI spectrum of 8vdA-10 upon incubation at 37 °C for 12 h in 10 mM citrate buffer (pH 4.0) showing the loss of 8-vinyladenine (M-161; the peak with a mass of 3105 is the $[M^+ + NH_4^+]$ peak).

Scheme 1: Fate of the Stem−Loop RNA, 8vdA-10, under Enzymatic and Nonenzymatic Conditions[a]

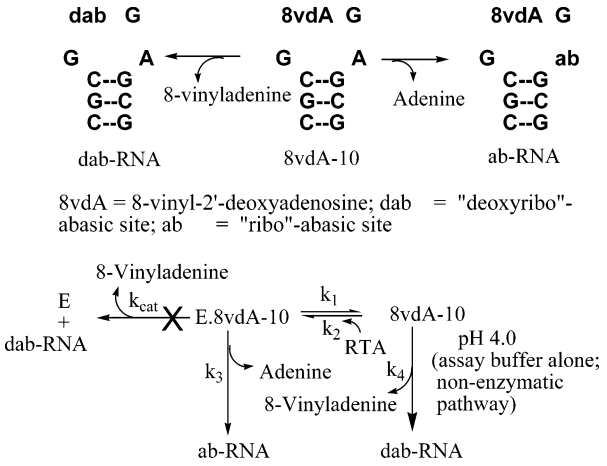

[a] 8vdA-10 binds to RTA ($K_i = k_2/k_1$) but 8-vinyladenosine is not hydrolyzed. Instead, adenine is released from the second site in the tetraloop (k_3). However, acid-catalyzed solvolysis in the pH 4.0 assay buffer results in depurination of 8-vinyladenine (k_4).

a rate for depurination at the second site while the first remains intact. In addition, the structure of the tetraloop with an abasic site ("GabGA") is different from an intact GAGA tetraloop. Thus, Chen's specificity constant comparison for the two adenosines is an approximation.

The release of adenine from 8vdA-10 could occur before or after the oligonucleotide is depurinated at the vinyl site. If 8vdA-10 binds to RTA and only deadenylation takes place, an accurate rate of depurination from the second site could be obtained, and if the binding constant of 8vdA-10 is similar to that of A-10, the second site depurination rate could be directly compared with the rate of release of adenine from the first site of A-10, thus providing the discrimination of specificities for the two sites. Scheme 1 shows the fate of 8vdA-10 upon binding to RTA. Literature suggests that RTA can cause both deadenylation of the first adenosine in a GAGA tetraloop and nonspecific deadenylation and deguanylation from other sites in stem−loop RNA (*33*). This study used synthetic 28-mer stem−loop RNA and 5S rRNA as substrates and reported deadenylation and deguanylation on the basis of denaturing gels. In our work, we determine the rates of depurination at individual sites.

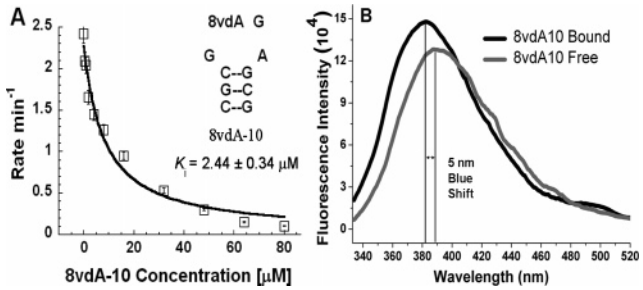

FIGURE 4: (A) Binding constant for binding of 8vdA-10 to RTA (K_i) determined from fits of initial rate data for the competitive substrate, A-10, with varied concentrations of 8vdA-10 to the equation $v = k_{cat}[S]/[[S] + K_m(1 + I/K_i)]$. (B) Fluorescence intensities of the free and bound forms of 8vdA-10. Binding of the RNA to RTA causes a 5 nm blue shift in the emission maximum.

Binding of 8vdA-10 to RTA: Competitive Inhibition and Fluorescence Studies. The dissociation constant of 8vdA-10 for RTA, K_i, was determined by using a 10-mer stem−loop RNA, A-10, as a competitive substrate. Under assay conditions where RTA satisfies initial rate conditions on A-10 and does not release either adenine or 8-vinyladenine (8-vA) from 8vdA-10, the competitive assay gives a K_i (Figure 4A) of 2.44 ± 0.34 μM for 8vdA-10, a value close to the K_m for A-10 (2.9 μM). Thus, 8vdA-10 binds as well as the A-10 substrate. However, despite its good binding, 8vdA is not hydrolyzed.

Fluorescence spectroscopy was also employed for a direct determination of the binding constant of 8vdA-10 and in exploring the base flipping mechanism. If 8vdA-10 were to adopt a hairpin tetraloop structure with a triple-purine stack and if RTA were to alter the torsion angle of the glycosidic bond of the vinyl nucleoside, it would disrupt this stack, make the vinyladenine more solvent-exposed, and increase the fluorescence of the "flipped-out" bound species through disruption of the quenching effect of the adjacent guanosines. However, a titration of increasing concentrations of RTA with a fixed concentration of 8vdA-10 caused an increase of only ~15% in fluorescence intensity at saturation (Figure 4B), making it difficult to determine the K_d of 8vdA-10 directly from the fluorescence experiment. The fluorescence of the bound species was blue-shifted by ~5 nm, suggesting an unstacking of the 8-vinyladenine (similar to the blue shift in the temperature dependence experiment discussed earlier). The small increase in fluorescence suggests that the flipped-

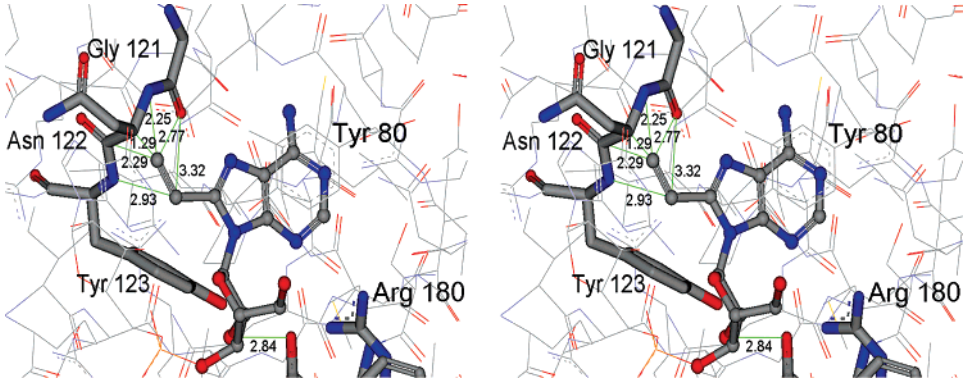

FIGURE 5: Stereoview of a docking model of 8-vinyladenine interactions in the active site of RTA created by superimposition on the coordinates of adenine in the crystal structure of RTA bound to the dinucleotide adenyl-3′,5′-guanosine (PDB entry 1APG). The vinyl moiety experiences steric clashes with the carbonyl oxygen of Gly121, the backbone amide and the α- and *β*-carbons of Asn122, and the backbone amide and the aromatic ring of Tyr123.

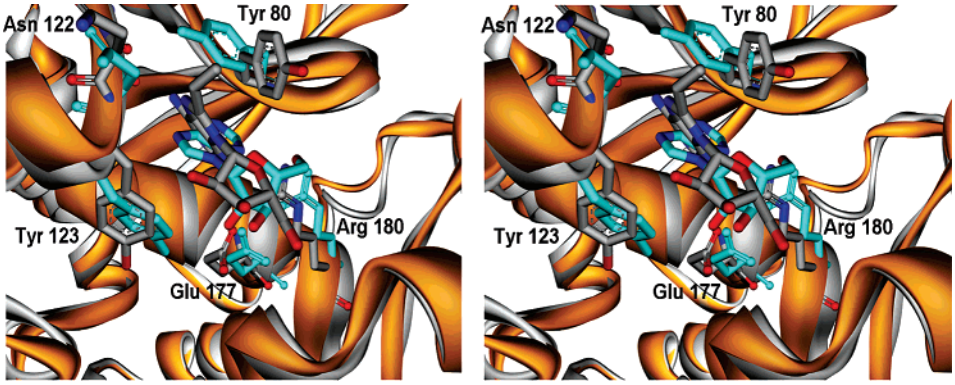

FIGURE 6: Stereoview of the superimposition of 300 ps simulated structures of RTA−ApG (cyan with ligand heteroatoms colored by atom type) and RTA−vApG (gray with heteroatoms colored by atom type) complexes. The C−N glycosidic bond dihedral rotates by ∼33° for the vinyladenosine which is accompanied by changes in side chain dihedral angles of Tyr80 and Tyr123. The 8-vinyladenine base avoids steric clashes with Asn122 and Tyr123 (compare with Figure 5).

out base becomes stacked between the two active site tyrosines (Tyr80 and Tyr123) which then efficiently quench its fluorescence. Thus, the overall change in fluorescence intensity upon binding is minimal since the vinyladenine moves from one stacked environment in the tetraloop to another in the hydrophobic RTA active site.

Binding of the Vinyladenine Moiety in the RTA Active Site: Molecular Dynamics Simulations. Attempts to crystallize either 8-vA or 8vAde with RTA were unsuccessful. Modeling of 8-vA in the crystal structure of RTA bound to adenine (Figure 5) indicates potential steric clashes with the α and *β* carbons of Asn122, the aromatic ring of Tyr123, and the carbonyl oxygen of Gly121. It has been suggested that RTA might use a base flipping mechanism to dock its target adenosine in the active site before depurination (*34*). In the uncomplexed structure of the sarcin ricin loop (SRL) RNA, the glycosidic bond of the susceptible adenosine, A_{4324}, is *anti* and the adenine base is involved in a triple-purine stack with the bases of the adjacent guanosine and adenosine. However, the crystal structure of ricin bound to a substrate analogue, formycin monophosphate (FMP), shows that the glycosidic bond is *syn* and the base stacks between two tyrosines, Tyr80 and Tyr123 (*19*). It is proposed that RTA recognizes the RNA with the susceptible adenosine in the *anti* conformation, flips it to the *syn* conformation, and finally catalyzes the hydrolytic reaction. Mély et al. (*15*) carried out a NOESY study and determined that both *syn* and *anti* conformations were present for the base in 8-vinyl-2′-deoxyadenosine. It is possible in the context of a RTA-bound structure that a C8 substituent forces the adenine ring to adopt an orientation (*syn* or *anti*) where steric factors preclude catalysis. Although competitive inhibition of A-10 hydrolysis by 8vdA-10 and the release of adenine from its second site both establish that this stem−loop RNA is an active site analogue, we carried out molecular dynamics simulations in an attempt to understand the surprising lack of catalysis.

The X-ray structure of RTA bound to the dinucleotide adenyl-3′,5′-guanosine, ApG (PDB entry 1APG) (*19*), was used as the starting model structure for the MD simulations. Two independent simulations were run, one with ApG and the other with the dinucleotide vApG where the adenosine is replaced with 8-vinyladenosine. The conformational binding mode for the adenine and ribose rings of adenosine is known from the X-ray structure. A comparative analysis of the simulated RTA−ApG and RTA−vApG complexes was carried out to determine the origin of the differences in catalysis between adenosine and 8-vinyladenosine. MD simulations with ApG have been reported in the literature, and our ApG simulation model was in good accord with those results (*35*). The simulation structures averaged over 300 ps show dramatic differences between the bound orientations of adenine (in ApG) and 8-vA (in vApG) in the hydrophobic pocket of RTA (Figure 6). Residues lining this pocket include Tyr80 in a *β*-strand and Tyr123 in an α-helix

Table 2: Comparative Interaction Distances (angstroms) for Two Sets of Simulations[a]

			simulation distance (Å)			
			adenosine		2′-deoxyadenosine	
ricin		X-ray	RTA−ApG	RTA−vApG	RTA−dApG	RTA−vdApG
R180 NH2	**Ade O4′**	**5.4**	**5.2 ± 0.4**	**3.1 ± 0.2**	**3.5 ± 0.2**	**2.9 ± 0.2**
	Ade N3	3.7	4.0 ± 0.8	3.2 ± 0.3	3.0 ± 0.1	3.1 ± 0.2
R180 NH1	Ade N3	3.0	3.7 ± 0.6	3.0 ± 0.2	3.5 ± 0.4	3.4 ± 0.4
	Ade O4′	**5.0**	**5.2 ± 0.2**	**3.4 ± 0.2**	**4.2 ± 0.2**	**3.1 ± 0.2**
E177 OE1	Ade O2′	3.5	3.7 ± 0.8	7.3 ± 0.4	−	−
	Ade O4′	6.6	6.3 ± 0.7	6.1 ± 0.5	6.7 ± 0.4	5.6 ± 0.7
E177 OE2	Ade O2′	2.8	3.6 ± 0.8	7.4 ± 0.6	−	−
	Ade O4′	5.7	6.2 ± 0.7	5.7 ± 0.3	6.3 ± 0.4	5.6 ± 0.7
WAT323 O	Ade C1′	4.1	5.1 ± 0.4	4.7 ± 0.7	4.5 ± 0.3	4.5 ± 0.6
	Ade O2′	2.5	3.6 ± 0.5	5.1 ± 0.9	−	−
E177 OE2	R180 NH1	2.2	2.8 ± 0.2	2.7 ± 0.1	2.8 ± 0.2	3.0 ± 0.2
E177 OE1	R180 NH2	2.3	5.1 ± 0.5	5.7 ± 0.6	5.0 ± 0.3	5.0 ± 0.2

[a] The most significant differences (1−2 Å) between adenyl and 8-vinyladenyl dinucleotides come from the interaction of Arg180 with the sugar ring oxygen. In the case of the vinyl nucleosides, the guanidinium nitrogens of Arg180 are 2 Å closer to ribosyl O4′ in the ribo simulations and 0.6−1.1 Å closer in the deoxyribo simulations, suggesting stronger sugar−Arg180 interactions.

Table 3: Comparative Interaction Energies (kilocalories per mole) for Adenine and 8-Vinyladenine Dinucelotide Simulations[a]

		interaction energy (kcal/mol)					
		ApG			vApG		
interacting residues		van der Waals	electrostatic	total	van der Waals	electrostatic	total
adenine	R180	−0.9	−12.3	−13.2	0.1	−13.5	−13.4
	Y123	−2.9	−0.2	−3.1	−3.7	−1.0	−4.7
	Y80	−4.0	−2.2	−6.2	−6.2	−1.9	−8.1
ribose	**R180**	**−1.3**	**−2.2**	**−3.5**	**−1.4**	**−6.0**	**−7.4**
	E177	1.1	−14.2	−13.1	−0.4	−1.3	−1.7
ribose O4′	**R180 NCN**	**−0.2**	**−8.8**	**−9.0**	**−0.1**	**−18.9**	**−19.0**

		interaction energy (kcal/mol)					
		dApG			vdApG		
interacting residues		van der Waals	electrostatic	total	van der Waals	electrostatic	total
adenine	R180	−0.02	−12.3	−12.3	−0.1	−12.9	−13.0
	Y123	−1.8	−1.9	−3.7	−2.7	−0.2	−2.9
	Y80	−4.7	−1.5	−6.2	−6.0	−1.8	−7.8
ribose	**R180**	**−1.8**	**−4.5**	**−6.3**	**−1.5**	**−8.8**	**−10.3**
	E177	−0.1	−0.1	−0.2	−0.2	−0.2	−0.4
ribose O4′	**R180 NCN**	**−0.3**	**−13.7**	**−14.0**	**−0.1**	**−19.5**	**−19.6**

[a] The most significant energetic differences (up to 4 kcal/mol) between adenyl and 8-vinyladenyl dinucleotides come from the interaction of Arg180 with the sugar ring oxygen. The isolated energetics between the guanidinium nitrogens and sugar O4′ are also highlighted.

and these are conserved in related enzymes. Their spatial disposition is coupled with the structural changes that accompany base binding. In particular, the backbone and side chain dihedral angles of Tyr80 undergo transitions that accompany the change in the dihedral angle of the C−N glycosidic bond in adenosine and 8-vinyladenosine. This dihedral angle governs the orientation of base binding in the active site. As shown in Figure 5, the hydrophobic pocket of RTA is tight so that the introduction of the vinyl substituent onto C8 of adenosine would result in several steric clashes if it was bound in the same orientation as the adenine ring in the X-ray structure, 1APG. The 300 ps MD simulation of vApG shows that these steric factors indeed play a major role since the glycosidic bond torsion in vinyladenosine rotates by 33° compared to bound adenosine. This allows the vinyl moiety to be accommodated such that steric clashes with residues Gly121, Asn122, and Tyr123 are avoided (see Figure 6). The dihedral angles that orient the aromatic rings in the two tyrosines change significantly to accommodate the vinyladenine in the most favorable and least sterically hindered orientation. The side chain dihedral angle of Tyr123 rotates from 150° in ApG to 82° in vApG, and that of Tyr80 changes from 82° to −177°. It is clear from the MD simulation that both the 8-vinyladenine and the catalytic site undergo conformational changes from both the crystal structure and the simulation structure of the RTA−ApG complex. Apart from the differences in stacking, the electrostatic interaction of Arg180 with N3 of the base is preserved in both adenosine and 8-vinyladenosine. However, for 8-vinyladenine, the contacts of N6 with Gly121 and Val81 and of N1 with Val81 are also weakened, suggesting that stacking is the dominant force for binding. It must be noted, however, that the simulation structure of ApG also shows several changes in the active site compared to its crystal structure. Nevertheless, these are not as dramatic as those seen for accommodation of the vinyladenine. The observed differences between the simulation structure and the X-ray structure are a result of the optimization of nonbonded interactions (electrostatic and van der Waals). In addition, as pointed out by Olson, ApG is a weak binding ligand such that multiple binding modes are possible (*35*).

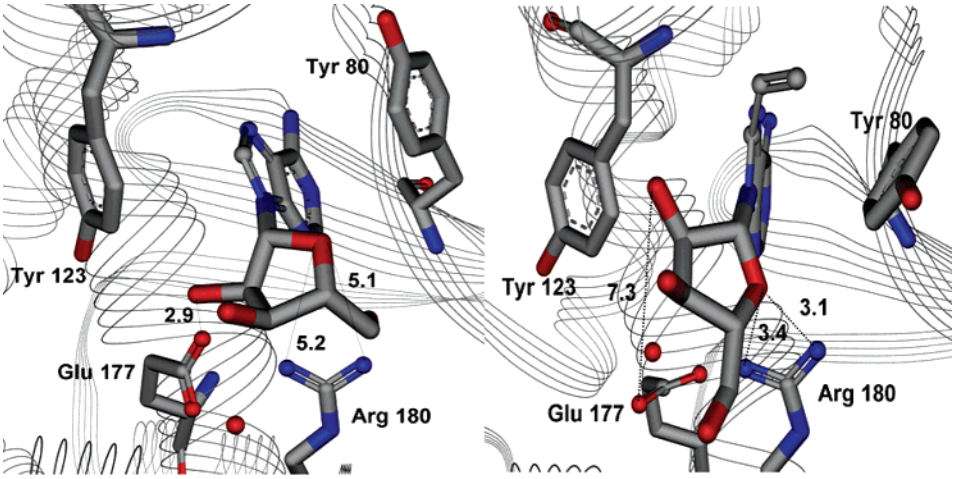

FIGURE 7: Active site interaction distances (angstroms) for 300 ps simulation structures of ApG (left) and the vinyl dinucleotide, vApG (right). Sterics reorganize the 8-vinyladenine base binding pocket and also reorient the ribosyl group. The guanidinium nitrogens of Arg180 in the RTA−vApG complex close in on the ribosyl O4′ by 1.8 Å for NH1 and 2.1 Å for the NH2, suggesting stronger sugar−Arg180 interactions. The 2′-hydroxyl−Glu177 interaction is also lost as this distance increases from 2.9 to 7.3 Å.

Having established an alternate binding mode for the 8-vinyladenine, we carried out an analysis of the interactions around the ribose ring. This analysis was compared with that of the adenosine ribosyl in the RTA−ApG complex. The ribose pucker configuration is 2′-*endo* for both adenosine and 8-vinyladenosine. However, the orientation of the ribosyl ring in the latter is dramatically different. In the ApG complex, the OE1 atom of Glu177 is 3.7 Å from the 2′-hydroxyl and 4.6 Å from C1′ of the ribose. In the vApG complex, these distances are 7.4 and 6.3 Å, respectively. Glu177 is a catalytic residue in the RTA active site that has been implicated in (a) an oxacarbenium ion stabilizing role at the transition state and (b) a general base role in abstracting a proton from a nucleophilic water molecule in the active site (*36*). Glu208 is another catalytic residue that has been implicated in catalysis (*36*). A weakening of interactions of the ribosyl group with these two residues may lead to a loss of oxacarbenium ion stabilization and thus a lack of catalytic efficiency. However, literature reports an E177A mutant that only lost catalytic efficiency by 20-fold over the wild-type RTA. In addition, the 2′-^{3}H KIE for hydrolysis of adenosine in a model 10-mer stem−loop RNA is reported to be 1.012 (*14*). It has been shown that polarization of the 2′-hydroxyl group leads to a higher value of the 2′-^{3}H KIE by a lengthening of the C2′−H2′ bond which in turn allows substantive hyperconjugative overlap between the σC2′−H2′ bond and the empty p-orbital on the anomeric carbon (C1′) of the oxacarbenium ion (*37*). Since this value is small in the case of RNA hydrolysis, it is likely that Glu177 in RTA does not operate via this mechanism. Instead, it may directly stabilize the oxacarbenium ion by electrostatic interaction. On the basis of these experimental results, it was thought that disruption of interactions with Glu177 would lead to a loss of catalytic efficiency but not complete abolishment of activity. However, the latter is observed in the case of the vinyl RNA, 8vdA-10.

A comparative analysis of distances and interaction energies of the RTA−ApG and RTA−vApG complexes then led to another interesting observation (see Tables 2 and 3 and Figure 7). The Arg180 nitrogens, NH1 and NH2, are ∼5−6 Å from the ribose ring oxygen in the case of both the X-ray and simulated structures of ApG. However, these distances are 3.4 and 3.1 Å, respectively, in the case of the simulated structure of the vinyladenyl compound, vApG. The analysis of interaction energies shows that the total energy for the ribose−Arg180 interaction is ∼4 kcal/mol lower for vApG than for ApG, suggesting a clear electrostatic stabilization of the ribosyl conformation in the vinyl dinucleotide.

Arg180 is a conserved residue in a family of ribosome-inactivating proteins, and mutations of this residue are severely detrimental to catalytic activity. A contribution of 4 kcal/mol can lead to an ∼1000-fold loss of catalytic activity [from $\Delta\Delta G = -RT \ln(k_1/k_2)$]. It is reasonable to assume that in the case of vApG, Arg180 plays a role in ground state stabilization (electrostatic attraction) of the ribose and/or transition state destabilization (repulsion) of the oxacarbenium ion.

Enzymes such as purine nucleoside phosphorylase (PNP) have been shown to exhibit coupled protein and substrate motion such that the purine 5′-hydroxyl and ribose ring oxygen and the nucleophile phosphate oxygen form a repulsive environment that promotes the lone pair of electrons to push from the ring oxygen to C1′, resulting in oxacarbenium ion formation (*38*). In the case of the RTA−vApG complex, coupled motion of protein and substrate allows the vinyladenine base to bind in an altered orientation. Coupled protein and ribose motion then brings the Arg180 into the proximity of the ribose ring oxygen. This would (1) serve to stabilize the ribose in the ground state but (2) be destabilizing for oxacarbenium ion formation and (3) result in loss of catalytic activity.

Thus, the entropic cost of organizing the 8-vinyladenine in the active site is coupled with the change in ribosyl orientation. The simulation model provides a rationale for the observation that 8vdA-10 binds to RTA but is not hydrolyzed. Although the simulation involves only a dinucleotide, similar changes in ribosyl geometry in the case of the RTA-bound RNA structure can lead to a loss of catalytic activity. As pointed out by Pande et al., the unique feature of the GNRA class of tetraloops is a cooperative relationship between 3′-*endo* ⇌ 2′-endo and closed loop ⇌ open loop transitions (*39*). The 2′-*endo* pucker modes expand the loop backbone and allow extension of the base away from the loop. It is reasonable to assume that in the dynamic

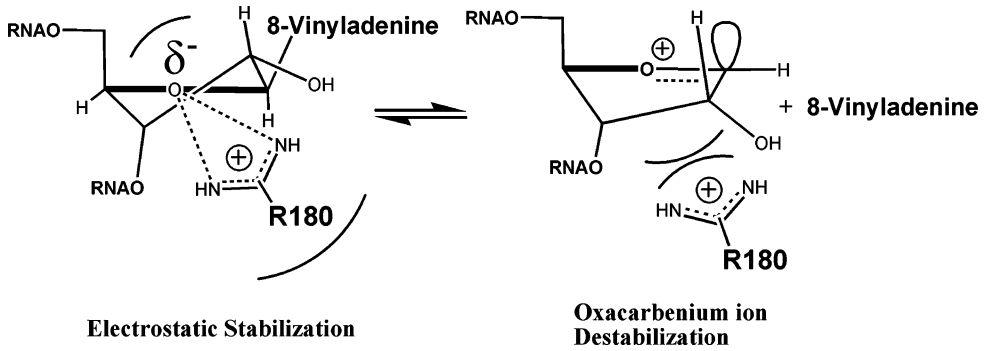

FIGURE 8: Model to explain the lack of catalysis by RTA of the 8-vinyladenyl-substituted RNA, 8vdA-10. Dynamics simulations predict Arg180 within 3 Å of the ribose 4′-oxygen. The consequence of this could be electrostatic stabilization of the ground state such that the formation of the oxacarbenium ion is destabilized and the reaction stalled.

open loop conformation with the depurination site base flipped out, changes in ribosyl geometry similar to those observed in the dinucleotide structure, vApG, can also be allowed in the larger RNA structure without a significant distortion of the orientations of the RNA chain on the 5′- and 3′-sides of the vinyladenosine. This also seems plausible given the 1 Å expanded backbone of the 8vApG (5′-O−3′-P distance of 5.6 Å) compared to the ApG structure.

MD simulations were also carried out for the 2′-deoxyadenylguanosine (dApG) and its vinyl counterpart, 8-vinyl-2′-deoxyadenylguanine (vdApG). The binding of the vinyladenine base involves a similar motion of Tyr80 (side chain dihedral angle changes from 81° to 177°) and Tyr123 (side chain dihedral angle changes from 92° to 85°) as described in the ribose case. The N−C glycosidic bond torsion angle (O4′−C1′−N9−C4) rotates from 31° in dApG to −27° in vdApG. The lack of catalysis in the case of the 2′-deoxy-8-vinyladenosine can again be rationalized on the basis of similar observations that Arg180 forms a strong electrostatic interaction with the deoxyribose ring oxygen in vdApG but not in dApG (energy difference of ∼4 kcal/mol). The Arg180−deoxyribose interaction is similar to the one observed with ribose. Thus, both sets of simulations show the same trends. Another interesting observation is that the geometry of the deoxyribosyl ring is 3′-*endo* for vdApG whereas it is 2′-*endo* for dApG. The interaction distances and energies are listed in Tables 2 and 3, respectively. Details of the simulation have been included in the Supporting Information (Figure S2 and Table S1).

Our MD simulations point toward an interesting mechanism by which RTA maintains its specificity for hydrolyzing adenosine. The hydrophobic pocket can bind a variety of base analogues (*11*) and is also involved in leaving group activation, but not all molecules that bind are hydrolyzed. Thus, it is likely that in the RTA−8vdA-10 structure, Arg180 is destabilizing for oxacarbenium ion formation, resulting in a nonproductive complex. This scenario is reminiscent of transition state destabilization in the DNA repair enzymes by 2′-fluoro-substituted nucleosides which form nonproductive complexes (*40*). Our theory about the lack of catalysis of 8vdA-10 by RTA thus invokes both steric and electronic factors. The alteration in 8-vinyladenine binding is coupled with the reorientation of ribose and deoxyribose rings (in vApG and vdApG, respectively) such that the interaction of Arg180 with the sugar ring oxygen is only observed in the vinyl nucleoside simulations. Figure 8 shows a schematic model for these observations.

Characterization of the Release of Adenine from the Second Site of the Tetraloop of 8vdA-10. RTA-catalyzed adenine release for 8vdA-10 was found to be slow with a k_{cat} of 0.023 ± 0.004 min^{-1}, a K_m of 205 ± 64 μM, and a k_{cat}/K_m of 2.03 ± 0.03 M^{-1} s^{-1} (see Figure S3A of the Supporting Information). Chen et al. determined the k_{cat}/K_m for the hydrolysis of stem−loop 10-mer RNA, A-10, to be 1.7×10^4 M^{-1} s^{-1} and the k_{cat} and K_m to be ∼4 min^{-1} and 4.1 μM, respectively (*12*). A comparison of the k_{cat}/K_m of A-10 with 8vdA-10 indicates that the recognition of the second adenosine in the tetraloop by RTA is ∼8000-fold weaker than that of the first site.

Since the specificity of RTA for the first adenosine is much higher than the second, other depurination events follow the first one. The conformation of the tetraloop changes once the first adenosine is cleaved, resulting in altered susceptibility for the second adenosine. As described above, Chen et al. observed a k_{cat} of ∼0.46 min^{-1} for release of the second site adenine from dR-10, a substrate that was abasic in the primary site. This rate is ∼20-fold faster than that observed for release of adenine from 8vdA-10 (which contains 8vdA at the primary site).

Release of adenine from the second adenosine on the tetraloop of 8vdA-10 suggests binding to RTA in two modes. One positions the 8-vA (8-vinyladenine) in the depurination site using the normal stem−loop geometry, and another reverse-disposes the 8-vA and the adenine by a 180° rotation of the tetraloop with respect to the catalytic site. Stem−tetraloop structures such as 8vdA-10 are known to be thermodynamically stable. However, it is possible that stem slippage could also alter loop structure. We calculated the secondary structures of the related 10-mer stem−loop molecule A-10 with mFold (version 2.3; structure calculated in 1 M NaCl at 25 °C) (*41*) and RNAshapes (*42*). An alternate geometry was found that results from slippage of two residues in the stem such that the second adenosine can be positioned in the RTA catalytic site for depurination. This alternate structure, TL2 (with a tetraloop, two base pairs, and a two-residue overhang), is 6.1 kcal/mol higher in energy than the most stable structure with the tetraloop and three base pairs, TL1 (Figure 9). However, the difference in the catalytic rates of depurination at the two sites [calculated using the expression $\Delta\Delta G^{TS} = -RT \ln(k_1 h/k_B T)/-RT \ln(k_2 h/k_B T)$ where k_1 and k_2 are the catalytic rate constants at the two sites] is ∼3.1 kcal/mol which is smaller than the barrier to interconversion between TL1 and TL2. Thus, the direct recognition of a slipped structure by RTA or an

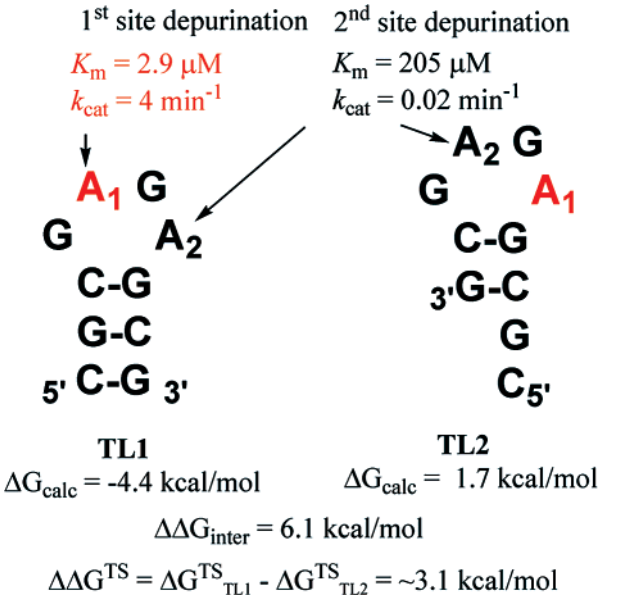

FIGURE 9: Substrate slippage model for RTA catalysis at the second adenosine site in the tetraloop. Two possible stem−tetraloop structures of A-10 calculated with the programs mFold and RNAshapes are shown. The barrier to interconversion between TL1 and TL2 in solution is higher than the difference in transition state energies for catalysis at the two sites.

enzyme-promoted slippage is unlikely. Disruption of base pairs and rearrangement of secondary structure on the enzyme are likely to be more energetically demanding than in solution. A simple 180° rotation of the tetraloop more easily explains both the high K_m and low rate of turnover at the second site.

Crystal structures of RTA bound to small molecules such as adenine and formycin monophosphate (*19*) or simulation models of hexamer, CGAGAG (*35*), indicate a single site for adenine depurination. Binding of 8vdA-10 gives a K_i of 2.4 μM which is a dissociation constant with respect to A-10 (K_m = 2.9 μM). This thermodynamic constant represents similar binding of 8vdA-10 and A-10. However, in adenine hydrolysis at the second site, the K_m of the vinyl RNA is 205 μM. Slow substrates of RTA are known to be in thermodynamic equilibrium; thus, K_m is also a dissociation constant. Therefore, adenine depurination of 8vdA-10 likely involves binding of the stem−loop structure in a 3′ → 5′ orientation opposite to that of A-10. Kinetic data with 8vdA-10 indicate that the catalytic specificity (k_{cat}/K_m) for the first adenosine in a 10-mer stem−tetraloop substrate is almost 3 orders of magnitude more favorable than that of the second site.

It is not clear if second-site deadenylation is physiologically relevant. However, our observations are relevant to inhibitor design in that it may be desirable to include nonhydrolyzable adenine isosteres at two sites in the tetraloop. Depurination reactions can occur in the same active site as a result of recognition of multiple conformations of the tetraloop. Catalytic rate efficiency at the two sites can be tested more directly on shorter cyclic versions of tetraloops which lack stems. Preliminary results comparing the K_i of a cyclic tetraloop analogue with the K_m for its second-site deadenylation suggest that the binding affinity of RTA for the second site adenosine is ~15-fold lower than the first (*43*). This difference is ~100-fold in the case of the stem−loop substrate, 8vdA-10, and suggests that the stem plays a role in the directionality of binding (5′ → 3′ vs 3′ → 5′).

Synthesis and Physicochemical Characterization of 8-Vinyladenine. Characterization of 8-vinyladenine has not been previously reported (*44*). A standard of 8-vinyladenine was synthesized for accurate quantitation of the hydrolytic rate of this novel nucleobase with the parent RNA. The precursor, "**1**", was treated with triethylamine in methanol (24 h at room temperature) to remove the formamidine followed by 15% dichloroacetic acid in dichloromethane for 3 h to remove the 5′-dimethoxytrityl group and cleave the glycosidic bond in one step (see the inset of Figure 10). The product was purified on a semipreparative C18 reverse phase column. The identity of the product was confirmed by ^{1}H NMR and ESI mass analysis in the negative mode.

Absorption spectra of known quantities of 8-vinyladenine were recorded to determine its extinction coefficient. The λ_{max} was 275 nm, and the absorption profile was broad with a spectral maximum between 270 and 290 nm. The millimolar extinction coefficient, ϵ, was determined to be 8.33. 8-vA was also characterized as a fluorophore (see Figure 2 and Table 1). As described earlier, the λ_{em} was 378 nm. The quantum yield, ϕ, was determined to be 0.37 relative to tryptophan (ϕ = 0.14) (*45*) and 0.33 relative to 2-aminopurine (ϕ = 0.66) (*27*). These determinations were made on absorbance-matched samples in water at pH 7.0 and 25 °C. The extended conjugation of 8-vinyladenine makes it a better leaving group than adenine. However, activation of adenine as a leaving group by RTA is proposed to occur via protonation of N7 and/or possibly N3. We were interested in determining the effect of the vinyl group on the pK_a values of these ring nitrogens and therefore on leaving group activation. ^{1}H NMR was used to follow the change in chemical shift of the vinyl CH═CH$_2$ proton and the proton at C8 of the purine ring with pH (Figure 10). The former is sensitive to changes in the environment of N9 and the latter to N1 or N3, neither of which is distinguished in this experiment. The NMR titration data were fitted to a biphasic pK_a equation with two pK_a values. The pK_a for N9 of 8-vA was found to be 9.5 and that for the N1−N3 system to be 4.6. These numbers are similar to those of adenine with a pK_a of 9.8 for N9. Thus, introduction of the vinyl group reduces the pK_a at N9 by only ~0.2−0.3 unit.

Since the pK_a of N7 cannot be determined from the NMR experiment, equilibrium geometries of 2′-deoxyadenosine (dAde) and 8-vinyl-2′-deoxyadenosine were optimized using the B3LYP/6-31G(d,p) level of theory with Gaussian 03 (*46*). The atomic electrostatic potential (ESP) charges using the Merz−Singh−Kollman (MK) scheme were computed at the same level of calculation. Charges at N7 in the two molecules were similar (−0.563 and −0.559, respectively), suggesting that the pK_a at N7 might also be similar (Figure S4 of the Supporting Information). The pK_a data and charge calculations along with the dynamics simulations suggest that steric factors enforced by the vinyl group orient the ribosyl group such that electronic factors from the enzyme then stabilize the ground state. Thus, electronic properties (of adenine and 8-vA) alone do not bring about the observed difference in catalysis of A-10 versus 8vdA-10.

The similarity between the K_d of 8vdA-10 and the K_m of A-10 (also a dissociation constant) suggests that binding is driven by extended structural contacts over the stem−loop

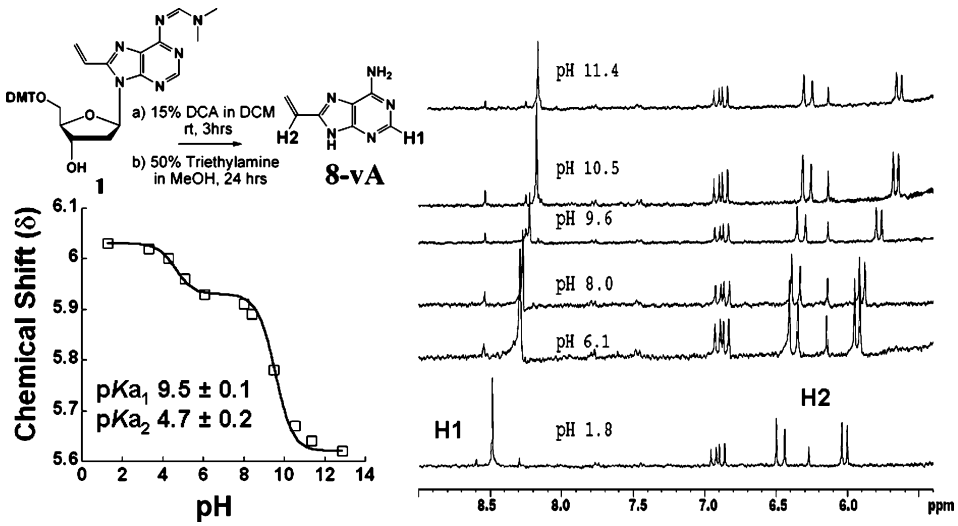

FIGURE 10: Determination of the pK_a of N9 in 8-vinyladenine by ^{1}H NMR. Data fitting is described in the text. The chemical shifts of the vinylic proton, H2 (doublet), in the 6 ppm region and that of the ring proton, H1 (singlet), in the 8.5 ppm region report on two protonation events, hence the biphasic curve. The inset shows the synthesis of 8-vinyladenine (8vA). Prolonged treatment of the dimethoxytritylated precursor nucleoside, **1**, under acidic conditions effected the removal of the DMT protecting group as well as cleavage of the glycosidic bond. The N6 protection was removed under basic conditions, and the final compound was purified by reverse phase HPLC.

structure (electronic and hydrophobic), whereas catalysis is driven by optimization of electronic interactions (such as H-bonding) with both adenine and ribose at the transition state. Nonenzymatic hydrolysis of 8-vA from 8vdA-10, albeit slow, confirms that it is an activated leaving group. Among the host of transition state analogue inhibitors designed for RTA, only those with small hydrophobic leaving groups (such as phenyl) bind more tightly than those with adenine analogues designed to provide a better pK_a match (*11*). This suggests that the high specificity of the RTA active site is due to efficient recognition of subtle electronic and steric properties of the RNA molecules. The extreme specificity of RTA is reflected in its hydrolysis of a single adenosine in the milieu of adenosines in ribosomal RNA.

Rate of Nonenzymatic Release of 8-Vinyladenine from 8vdA-10. The change in the fluorescence intensity of 8vdA-10 was recorded as a function of time to determine the rate of 8-vA release. As mentioned earlier, the fluorescence intensity of the 8-vinyladenine in stem−loop RNA is dependent on the conformation of the tetraloop.

A 270-fold reduction in fluorescence intensity is observed when 8vdA is incorporated in the tetraloop of 8vdA-10. Release of 8-vA from 8vdA-10 was followed at pH 4.0 (10 mM citrate buffer) over 10 h. The rate constant (k_4 in Scheme 1) was 6×10^{-5} nmol/min. This rate is ~300-fold slower than the rate of release of adenine from the second site ($k_{cat} \sim 0.02$ min^{-1}; k_3 in Scheme 1) by RTA. The rate constant was determined from the change in fluorescence intensity of a 5 μM solution of 8vdA-10 at 25 °C (Figure 11).

Control experiments in a pH 7.6 buffer showed a <1% change in fluorescence intensity over 12 h, consistent with a stable tetraloop conformation and an insignificant hydrolytic rate. A comparison of the nonenzymatic 8-vinyladenine release rate versus enzymatic adenine release established that deadenylation of the tetraloop occurred with 8-vinyl-2′-deoxyadenosine still intact in the loop. A negligible change in fluorescence intensity was observed during the release of adenine from the second site in the tetraloop. It must be noted

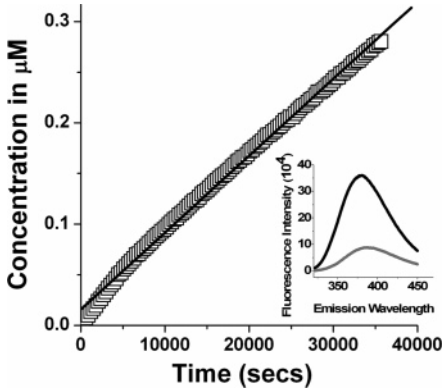

FIGURE 11: Continuous release of 8-vinyladenine from the stem−loop oligomer, 8vdA-10, over 10 h in 10 mM citrate buffer (pH 4.0). The rate constant was derived from a fit to the equation $k = (1/\Delta\alpha)(\Delta F/\Delta t)$, where $\Delta F/\Delta t$ is the rate in fluorescence units per second and $\Delta\alpha = F_{tot}/[S]_{tot}$, where F_{tot} is the total fluorescence increase for 100% conversion of substrate ($[S]_{tot}$) to product. Excitation was set at 305 nm, and the emission spectrum was recorded in the 320−450 nm range.

that since the quantum yield of 8-vA is 130-fold greater than that of 8-vinyl-2′-deoxyadenosine within the RNA, it is possible to determine very small release rates.

Kinetics of A-14 Turnover by Pokeweed Antiviral Protein (PAP). Of the various RIPs, pokeweed antiviral protein (PAP) isolated from the leaves of *Phytolacca americana* has been shown to have a broad RNA substrate specificity relative to the GAGA tetraloop specificity of RTA (*47*). Given this promiscuity of PAP, we decided to test its catalytic activity on 8vdA-10. Rajamohan et al. (*48*) showed that both wild-type and recombinant PAP were able to deadenylate *E. coli* 23S and 16S rRNA in 25 mM Tris-HCl at pH 7.8. The same pH conditions were used to test 8vdA-10 as a PAP substrate. Before we were able to test the hypothesis of 8vdA-10 turnover by PAP, it was necessary to investigate the depurinating ability of PAP on a small stem−loop SRL RNA mimic, A-14.

PAP was heat treated to remove the nonspecific glycosidase/nuclease activity while retaining the RNA *N*-glycosidase activity (*49*). Adenine release was detected upon incubation of A-14 with a commercial source wild-type PAP at pH 7.8 (25 mM Tris-HCl buffer). The K_m for A-14 was 220 ± 20 μM, and the k_{cat} was 2.9 ± 0.2 min^{-1} (Figure S3B of the Supporting Information). For comparison, the K_m and k_{cat} for A-14 hydrolysis by RTA are 8.1 μM and 219 min^{-1}, respectively (*12*). It is remarkable that RTA has optimal activity at pH 4.0 but is inactive at neutral pH for hydrolysis of small stem−loop RNA, whereas PAP can operate at neutral pH, albeit not efficiently. Having established that A-14 is a substrate of PAP, we tested its ability to hydrolyze 8vdA-10 under neutral-pH conditions.

Hydrolysis of 8vdA-10 by PAP. Incubation of 8vdA-10 with PAP at pH 7.8 (25 mM HEPES buffer) resulted in release of both adenine and of 8-vinyladenine. Adenine release occurred at an initial rate of 0.018 min^{-1}. Kinetic characterization of binding of 8vdA-10 to PAP indicated a K_m of >300 μM for this substrate. The rate of release of 8-vinyladenine, measured by the continuous change in the fluorescence intensity of a 5 μM solution of 8vdA-10 on incubation with 1 μM PAP, was determined to be ~1.6 × 10^{-3} min^{-1} which is 10-fold lower than the rate of release of adenine from the second site. These results establish that 8-vA is released by PAP, but not as efficiently as adenine from the second site. The RTA active site is highly stringent in comparison and does not catalyze 8-vA release.

CONCLUSIONS

We have designed a new RNA−DNA hybrid substrate analogue, 8vdA-10, that binds to RTA with a K_i value similar to the K_m of the small stem−loop RNA 10-mer, A-10. Despite having an activated leaving group, the N-glycosidic bond of the 8-vinyl-2′-deoxyadenosine in the RNA is not cleaved by RTA. Dynamics calculations suggest that steric factors cause the nucleoside to bind in an orientation where the enzyme destabilizes the formation of the oxacarbenium ion and thus precludes catalysis. However, adenine is released from the second site of 8vdA-10. This deadenylation rate is 2 orders of magnitude slower than that measured for depurination of the first site adenosine in A-10. The binding affinity of 8vdA-10 for the catalytic site that results in the second-site depurination is ~100-fold lower than that for the first, indicating an alternate binding geometry for the modified vinyl RNA. The new stem−loop analogue described here thus allows a comparison of the enzymatic specificities for the two adenosines in a tetraloop RNA structure since the first site is still intact when the second-site depurination occurs. The results with PAP suggest that second-site depurination can also occur at neutral pH. Glycosidic bond scission at a specific site on the 28S rRNA by ribosome binding proteins is stringent under physiological conditions. However, the release of multiple adenines from truncated stem−loop RNA analogues suggests that nonhydrolyzable adenine isosteres at both sites in the GAGA tetraloop might be of interest for inhibitor design. Our study complements the work of Mély et al. and shows that the 8-vinyl moiety is a useful fluorophore system that can be exploited further in the study of protein−RNA complexes.

ACKNOWLEDGMENT

We thank Mr. Matthew Sturm for valuable discussions and Dr. Steven D. Schwartz for providing the computing resource for the molecular dynamics simulations.

SUPPORTING INFORMATION AVAILABLE

Molecular dynamics simulations, determination of kinetic constants, and calculation of atomic charges. This material is available free of charge via the Internet at http://pubs.acs.org.

REFERENCES

1. Endo, Y., Chan, Y. L., Lin, A., Tsurugi, K., and Wool, I. G. (1988) The cytotoxins α-sarcin and ricin retain their specificity when tested on a synthetic oligoribonucleotide (35-mer) that mimics a region of 28S ribosomal ribonucleic acid, *J. Biol. Chem. 263*, 7917−7920.
2. Kudlicki, W., Kitaoka, Y., Odom, O. W., Kramer, G., and Hardesty, B. (1995) Elongation and folding of nascent ricin chains as peptidyl-tRNA on ribosomes: The effect of amino acid deletions on these processes, *J. Mol. Biol. 252*, 203−212.
3. Moazed, D., Robertson, J., and Noller, H. (1988) Interaction of elongation factors EF-G and EF-Tu with a conserved loop in 23S RNA, *Nature 334*, 362−364.
4. Endo, Y., and Tsurugi, K. (1988) The RNA N-glycosidase activity of ricin A-chain. The characteristics of the enzymatic activity of ricin A-chain with ribosomes and with rRNA, *J. Biol. Chem. 263*, 8735−8739.
5. Sandvig, K., and van Deurs, B. (2002) Transport of protein toxins into cells: Pathways used by ricin, cholera toxin and Shiga toxin, *FEBS Lett. 529*, 49−53.
6. Lord, J. M., Deeks, E., Marsden, C. J., Moore, K., Pateman, C., Smith, D. C., Spooner, R. A., Watson, P., and Roberts, L. M. (2003) Retrograde transport of toxins across the endoplasmic reticulum membrane, *Biochem. Soc. Trans. 31*, 1260−1262.
7. Eiklid, K., Olsnes, S., and Pihl, A. (1980) Entry of lethal doses of abrin, ricin and modeccin into the cytosol of HeLa cells, *Exp. Cell Res. 126*, 321−326.
8. Rich, V. (1992) Murderous experiments of Stalin's police chief, *New Sci. 135*, 8.
9. Remnick, D. (1992) *Washington Post*, April 21, D1.
10. Ler, S. G., Lee, F. K., and Gopalakrishnakone, P. (2006) Trends in detection of warfare agents Detection methods for ricin, staphylococcal enterotoxin B and T-2 toxin, *J. Chromatogr., A 1133*, 1−12.
11. Roday, S., Amukele, T., Evans, G. B., Tyler, P. C., Furneaux, R. H., and Schramm, V. L. (2004) Inhibition of ricin A-chain with pyrrolidine mimics of the oxacarbenium ion transition state, *Biochemistry 43*, 4923−4933.
12. Chen, X. Y., Link, T. M., and Schramm, V. L. (1998) Ricin A-chain: Kinetics, mechanism, and RNA stem-loop inhibitors, *Biochemistry 37*, 11605−11613.
13. Orita, M., Nishikawa, F., Kohno, T., Senda, T., Mitsui, Y., Yaeta, E., Kazunari, T., and Nishikawa, S. (1996) High-resolution NMR study of a GdAGA tetranucleotide loop that is an improved substrate for ricin, a cytotoxic plant protein, *Nucleic Acids Res. 24*, 611−618.
14. Chen, X. Y., Berti, P. J., and Schramm, V. L. (2000) Ricin A-Chain: Kinetic Isotope Effects and Transition State Structure with Stem-Loop RNA, *J. Am. Chem. Soc. 122*, 1609−1617.
15. Ben Gaied, N., Glasser, N., Ramalanjaona, N., Beltz, H., Wolff, P., Marquet, R., Burger, A., and Mély, Y. (2005) 8-Vinyl-deoxyadenosine, an alternative fluorescent nucleoside analog to 2′-deoxyribosyl-2-aminopurine with improved properties, *Nucleic Acids Res. 33*, 1031−1039.
16. Manfredini, S., Baraldi, P. G., Bazzanini, R., Marangoni, M., Simoni, D., Balzarini, J., and De Clercq, E. (1995) Synthesis and cytotoxic activity of 6-vinyl- and 6-ethynyluridine and 8-vinyl- and 8-ethynyladenosine, *J. Med. Chem. 38*, 199−203.

17. Segel, I. (1993) *Enzyme Kinetics*, Wiley Classics Library Edition, John Wiley & Sons, New York.
18. Lakowicz, J. R. (1999) *Principles of Fluorescence Spectroscopy*, 2nd ed., Kluwer Academic/Plenum Publishers, New York.
19. Monzingo, A. F., and Robertus, J. D. (1992) X-ray analysis of substrate analogs in the ricin A-chain active site, *J. Mol. Biol. 227*, 1136−1145.
20. Rutenber, E., Katzin, B. J., Ernst, S., Collins, E. J., Mlsna, D., Ready, M. P., and Robertus, J. D. (1991) Crystallographic refinement of ricin to 25 Å, *Proteins 10*, 240−250.
21. Brook, C. L., III, and Karplus, M. J. (1983) Deformable stochastic boundaries in molecular dynamics, *J. Chem. Phys. 79*, 6312−6325.
22. Brooks, B. R., Bruccoleri, R. E., Olafson, B. D., States, D. J., Swaminathan, S., and Karplus, M. (1983) CHARMM: A program for macromolecular energy, minimization, and dynamics calculations, *J. Comput. Chem. 4*, 187−217.
23. Jorgensen, W. L., Chandrasekhar, J., Madura, J. D., Impey, R. W., and Klein, M. L. (1983) Comparison of simple potential functions for simulating liquid water, *J. Chem. Phys. 79*, 926−935.
24. Brook, C. L., III, and Karplus, M. (1989) Solvent effects on protein motion and protein effects on solvent motion, *J. Mol. Biol. 208*, 159−181.
25. Ryckaert, J.-P., Ciccoti, G., and Berendsen, H. J. C. (1977) Numerical integration of the cartesian equations of motion of a system with constraints: Molecular dynamics of *n*-alkanes, *J. Comput. Phys. 23*, 327−341.
26. Alul, R. H., Singman, C. N., Zhang, G. R., and Letsinger, R. L. (1991) Oxalyl-CPG: A labile support for synthesis of sensitive oligonucleotide derivatives, *Nucleic Acids Res. 19*, 1527−1532.
27. Sproat, B., Colonna, F., Mullah, B., Tsou, D., Andrus, A., Hampel, A., and Vinayak, R. (1995) An Efficient Method for the Isolation and Purification of Oligoribonucleotides, *Nucleosides Nucleotides 14*, 255−273.
28. Ward, D. C., Reich, E., and Stryer, L. (1969) Fluorescence studies of nucleotides and polynucleotides. I. Formycin, 2-aminopurine riboside, 2,6-diaminopurine riboside, and their derivatives, *J. Biol. Chem. 244*, 1228.
29. Jucker, F. M., Heus, H. A., Yip, P. F., Moors, E. H., and Pardi, A. (1996) A network of heterogeneous hydrogen bonds in GNRA tetraloops, *J. Mol. Biol. 264*, 968−980.
30. Correll, C. C., Munishkin, A., Chan, Y. L., Ren, Z., Wool, I. G., and Steitz, T. A. (1998) Crystal structure of the ribosomal RNA domain essential for binding elongation factors, *Proc. Natl. Acad. Sci. U.S.A. 95*, 13436−13441.
31. Kenfack, C. A., Burger, A., and Mély, Y. (2006) Excited-state properties and transitions of fluorescent 8-vinyl adenosine in DNA, *J. Phys. Chem. B 110*, 26327−26336.
32. Chen, X. Y., Berti, P. J., and Schramm, V. L. (2000) Transition-State Analysis for Depurination of DNA by Ricin A-Chain, *J. Am. Chem. Soc. 122*, 6527−6534.
33. Tang, S., Xie, L., Hou, F., Liu, W. Y., and Ruan, K. (2001) Non-specific deadenylation and deguanylation of naked RNA catalyzed by ricin under acidic condition, *Biochim. Biophys. Acta 1519*, 192−198.
34. Yang, X., Gerczei, T., Glover, L. T., and Correll, C. C. (2001) Crystal structures of restrictocin-inhibitor complexes with implications for RNA recognition and base flipping, *Nat. Struct. Biol. 8*, 968−973.
35. Olson, M. A. (1997) Ricin A-chain structural determinant for binding substrate analogues: A molecular dynamics simulation analysis, *Proteins: Struct., Funct., Genet. 27*, 80−95.
36. Kim, Y., Mlsna, D., Monzingo, A. F., Ready, M. P., Frankel, A., and Robertus, J. D. (1992) Structure of a ricin mutant showing rescue of activity by a noncatalytic residue, *Biochemistry 31*, 3294−3296.
37. Singh, V., and Schramm, V. L. (2006) Transition-state structure of human 5′-methylthioadenosine phosphorylase, *J. Am. Chem. Soc. 128*, 14691−14696.
38. Nunez, S., Antoniou, D., Schramm, V. L., and Schwartz, S. D. (2004) Promoting vibrations in human purine nucleoside phosphorylase. A molecular dynamics and hybrid quantum mechanical/molecular mechanical study, *J. Am. Chem. Soc. 126*, 15720−15729.
39. Sorin, E. J., Engelhardt, M. A., Herschlag, D., and Pande, V. S. (2002) RNA simulations: Probing hairpin unfolding and the dynamics of a GNRA tetraloop, *J. Mol. Biol. 317*, 493−506.
40. Schaerer, O. D., and Verdine, G. L. (1995) A Designed Inhibitor of Base-Excision DNA Repair, *J. Am. Chem. Soc. 117*, 10781−10782.
41. Walter, A. E., Turner, D. H., Kim, J., Lyttle, M. H., Müller, P., Mathews, D. H., and Zuker, M. (1994) Coaxial stacking of helixes enhances binding of oligoribonucleotides and improves predictions of RNA folding, *Proc. Natl. Acad. Sci. U.S.A. 91*, 9218−9222.
42. Steffen, P., Voss, B., Rehmsmeier, M., Reeder, J., and Giegerich, R. (2006) RNAshapes: An integrated RNA analysis package based on abstract shapes, *Bioinformatics 22*, 500−503.
43. Sturm, M., Roday, S., and Schramm, V. L. (2007) Circular DNA and DNA/RNA hybrid molecules as scaffold for ricin inhibitor design. *J. Am. Chem. Soc. 129*, in press.
44. Lang, P., Magnin, G., Mathis, G., Burger, A., and Biellmann, J.-F. (2000) Synthesis of 8-(ω-hydroxyalkyl)-, 8-(ω-hydroxyalk-1-enyl)-, and 8-(ω-hydroxy-3-alk-1-ynyl)adenines using the *tert*-butyldimethylsilyloxymethyl group, a new and versatile protecting group of adenine, *J. Org. Chem. 65*, 7825−7832.
45. Kirby, E. P., and Steiner, R. F. (1970) Influence of solvent and temperature upon the fluorescence of indole derivatives, *J. Phys. Chem. 74*, 4480−4490.
46. Frisch, M. J., Trucks, G. W., Schlegel, H. B., Scuseria, G. E., Robb, M. A., Cheeseman, J. R., Zakrzewski, V. G., Montgomery, J. A., Jr., Stratmann, R. E., Burant, J. C., Dapprich, S., Millam, J. M., Daniels, A. D., Kudin, K. N., Strain, M. C., Farkas, O. J., Tomasi, B. V., Cossi, M., Cammi, R., Mennucci, B., Pomelli, C., Adamo, C., Clifford, S., Ochterski, J., Petersson, G. A., Ayala, P. Y., Cui, Q., Morokuma, K., Malick, D. K., Rabuck, A. D., Raghavachari, K., Foresman, J. B., Cioslowski, J., Ortiz, J. V., Stefanov, B. B., Liu, G., Liashenko, A., Piskorz, P., Komaromi, I., Gomperts, R., Martin, R. L., Fox, D. J., Keith, T., Al-Laham, M. A., Peng, C. Y., Nanayakkara, A., Gonzalez, C., Challacombe, M., Gill, P. M. W., Johnson, B., Chen, W., Wong, M. W., Andres, J. L., Gonzalez, C., Head-Gordon, M., Replogle, E. S., and Pople, J. A. (2003) *Gaussian 03*, revision B.04, Gaussian, Pittsburgh, PA.
47. Parikh, B. A., and Tumer, N. E. (2004) Antiviral activity of ribosome inactivating proteins in medicine, *Mini-Rev. Med. Chem. 4*, 523−543.
48. Rajamohan, F., Mao, C., and Uckun, F. M. (2001) Binding interactions between the active center cleft of recombinant pokeweed antiviral protein and the α-sarcin/ricin stem loop of ribosomal RNA, *J. Biol. Chem. 276*, 24075−24081.
49. Day, P. J., Lord, J. M., and Roberts, L. M (1998) The deoxyribonuclease activity attributed to ribosome-inactivating proteins is due to contamination, *Eur. J. Biochem. 258*, 540−545.

BI0621821